Available online at www.jrors.yazd.iau.ir

Journal Of Radar and Optical Remote Sensing and GIS

JRORS 3 (2022) 82–98

Application of ATER Data for Identification of Alteration Zone of XIV Anomalies Area, Bafq, Central Iran

Samira Bakhtiyari[a*], Mohammad Lotfi[b]

[a]*Department of Geology, Science and Research Branch, Islamic Azad University, Tehran, Iran*

[b]*Department of Geology, Tehran (North) Branch, Islamic Azad University, Iran and Research Institute for Earth Science, Geological Survey of Iran, Tehran, Iran*

Received 26 February 2022; Revised 26 May 2022; Accepted 17 August 2022

Abstract

We studied the applicability of data from the ASTER sensor for mapping hydrothermal alteration areas and lithological units associated with Kiruna type mineralization in arid and semi-arid regions. The XIV iron oxide anomalies in the Bafq provience in Central Iran was selected for a case study. The XIV anomalies occur in a northwest–southeast-trending fault zone that is characterized by the presence of a narrow zone of alteration–mineralization. Mineralogical evidences of Kiruna mineralization is mapped by spectral processing techniques. The alteration minerals in the XIV anomalies (the related iron oxide deposit) have been successfully detected by applying ratio images, relative band depth method, false color composite, minimum noise fraction, least square fit, pixel purity index techniques on ASTER imageries. Phyllic, argillic, propylitic, silicic alteration zones and in addition to areas of secondary Fe-oxide formation can be distinguished. Results indicates that ASTER data is capable of delineating alteration footprints of Kiruna mineral system in deposit scale exploration.

Keywords*:* Kiruna, ASTER, Alteration, Bafq, XIV Anomaly

1. Introduction

Ore deposits are often produced by fluid flow processes that alter the mineralogy and chemistry of the country rocks. This alteration can produce distinctive assemblages of minerals that vary according to the location, and the length of time over which the flow processes operated (Ferrier and Wadge 1996; Ferrier et al. 2002). It is possible to map the types of alteration on the exposed ground surface.

Remote sensing techniques are of valuable use in mapping hydrothermally altered minerals that have distinct absorption features (Hunt 1979). Multispectral remote sensing sensors provide detailed information on the mineralogy of different rock types of the earth's surface, and have been used by several scientists (Crósta and Moore 1989; Loughlin 1991; Abdelsalam et al. 2000; Rokos et al. 2000; Ferrier et al. 2002; Crósta and Filho 2003; Zhang et al. 2007; Gabr et al. 2010; Pazand et al. 2016; Mokhtari et al. 2016; Bhadra et al. 2016).

* Corresponding author Tel: +98-2188936295.
Email address: sbakhtiyare@yahoo.com, s.bakhtiyari@srbiau.ac.ir.

The multispectral satellite images have widly application for mineral exploration due to presence of key minerals of alteration zones. The advanced spaceborne thermal emission and reflection radiometer (ASTER) is an advanced multispectral satellite launched in orbit in December, 1999. ASTER covers a wide spectral region with 14 bands, from the visible to the thermal infrared with high spatial, spectral and radiometric resolution. The spatial resolution varies with wavelength: 15 m in the visible and near-infrared (VNIR), 30 m in the short wave infrared (SWIR), and 90 m in the thermal infrared (TIR) (Abrams and Hook 2000). ASTER diverse bands allow a wealth of minerals to be mapped: The three VNIR bands are important sources of information regarding absorption in transition metals (e.g. Fe). In six SWIR bands carbonate, hydrate and hydroxide mineral spectra display molecular absorption features. Rock-forming minerals like quartz display fundamental molecular absorption features in the TIR wavelength region (Rowan and Mars 2003)

In an article, the information about gold exploration in the Sanandaj-Sirjan region is discussed, and in this research, ASTER is used to map hydrothermal alteration minerals and better detect geological structural features related to orogenic gold in the region, and it is a fast tool. and cost-effectiveness to initiate a comprehensive geological and geochemical exploration program in the study area and elsewhere in similar areas (Sheikhrahimi, et al, 2019).

In a study in the Takab region located in the northwest of Iran, the data of the advanced space thermal and reflection radiometer have been evaluated for mapping gold and base metal mineralization through alteration mapping with two different methods for argillic and siliceous alteration mapping (Moore et al (2008).

In another research in the Sinai region of Egypt to investigate uranium by means of remote sensing data and GIS tools were used to determine the location and mapping of these mineral deposits. Minerals were identified and mapped using feature-oriented principal component selection (Crusta technique) on ASTER image (Aita & Omar (2021).

In another research to obtain surface reserves of mineral resources presents an integrated approach for deep mineral exploration in some promising areas of Gabal (G) Semna region, Eastern Desert (ED) Egypt (Eldosouky et al, 2021)

Mahmoud Abd E et al., in a research in Um Balad region, a part of Arabian Nubian Shield (ANS) by means of automatic line extraction method using visible and near infrared bands of ASTER was used to produce line density map of mineral (Hegab et al,2022).

In another study, the Neuro-Fuzzy-AHP (NFAHP) technique was used to combine remote sensing (e.g. ASTER transformation mineral image maps) and geological datasets (e.g. lithology map, geochromological map, structural map and Geochemistry) developed to identify high potential areas of volcanic massive copper sulfide (VMS) mineralization in Sahlabad mining area, east of Iran. Argillic, phyllic, propylitic, and gasan alteration zones were identified in the study area using band ratio methods and selected principal component analysis (SPCA) for ASTER VNIR and SWIR bands. As a result, the Neuro-Fuzzy-AHP (NFAHP) technique shows high reliability for copper exploration in Sahlabad mining area, it can be extrapolated to other areas for the identification stage of mineral exploration (Shirazi et al, 2022).

The current study aims to investigate and characterize the footprints of XIV anomalies Kiruna mineralization through a series of mineral maps extracted from ASTER satellite imagery. The main purpose of this research is to detect, discriminate of major alteration minerals in the XIV anomalies area with iron oxide (Cu-U-Au-REE) deposit alteration minerals, as suggested by Hitzman et al. (1992) and Hitzman (2000). This paper does not intend to review the use of remote sensing for iron exploration at this area. We show that pervasive hydrothermal ore-forming processes have played the most important role in producing the XIV iron deposit and in other parts of the Ariz sheet.

1.2. Geological Setting

The origin of the Bafq iron oxide deposits related to igneous rocks has been the subject of a long-standing and heated debate for the last hundred years (Frietsch 1978; Nyström 1994; Borook et al.

1998). Different ore genesis models have been proposed for these ore deposits.

These deposits are usually composed of magnetite-hematite-fluorapatite with varying amounts of alkali amphiboles. They occur worldwide and range in size from large high-grade orebodies to small dikes and veinlets. They are usually found in cambrian volcano-sedimentary sequence (also known as Saghand formation) associated with number of felsic and mafic intrusions. These ore bodies are commonly associated with pervasively altered rhyolitic tuffs and sandstones. Among these deposits, the so-called Kiruna-type ores have attracted the most attention.

2. Material and Methods

The XIV Anomalies is located between 55˚28', 55˚33' longitude and 32˚00', 32˚08' latitude in south of Bafq province (eastern of 1:100000 Ariz sheet). Based on 1:100000 geological map of Ariz, the most impressive lithological features in studied area are the volcanic and plutonic stones with acidic to basic combination. these features are included andesite, andesibasalt, dacite and rhyodacite. There are leucogranite, aplite, Gabbro and diorite in north, east and south and mafic dikes in west and chertydolomite in eastern of investigated area.

Hematitation, limonitation, propylitic, phyllic and argillic alterations are seen in central parts that have been formed in north west – south east trend in studied area. Volcanic rocks have specific conditions. For example, ferrous ore formed along fracture in tectonic environment. Based on 1:100000 geological map of Ariz, three NW-SE faults have been seen. According to our results, around the faults, alteration and ferrous fluid have been observed (Fig1)

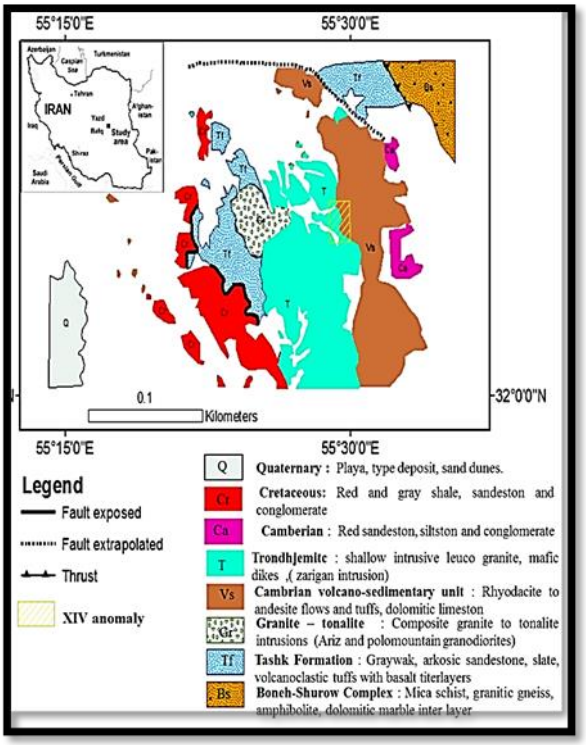

Figure 1. Simplified geological map of the Ariz 1:100000 (Modifiedafter Forster and Jafarzadeh 1992; Haghipour, 1977; Ramezani and Tucker, 2003)

Data format (HDF) was used for this research. To remove atmospheric and topographic effects from ASTER SWIR and ASTER VNIR data, was used (Green et al. 1988). The resulting data could be

assumed to be more representative of the soils or lithologies of the exposed areas than the unprocessed data. Hence, a spectrum generated from data treated using the log-residual method will be more closely comparable to its corresponding library spectrum. Because the log-residual algorithm reduces noise from topography, instruments, and sun illumination, the processed ASTER SWIR and ASTER VNIR data will allow comparison of the synthesized spectrum with those from the library.

Many image analysis and processing techniques can be used to interpret the spectral data. In this paper, several of these approaches are used, including the normalized difference false color composite (FCC), ratio image, relative band depth (RBD), minimum noise fraction (MNF), spectral angle mapper (SAM), principal component analysis (PCA) and pixel purity index (PPI) and least square fit (Ls-Fit) methods were used on ASTER data for separation of alteration zones.

3. Results

3.1. Kiruna Mineralization

Kiruna ore deposits have high economic potential and include a wide spectrum of sulphide-deficient low-Ti magnetite and/or hematite ore bodies of hydrothermal origin (breccias, veins veins, stockworks or massive lenses) with polymetallic enrichment (Cu, Au, Ag, P, U, REE, etc.) which are genetically associated (either proximal or distal) with large scale calcalkaline or alkaline magmatism (Hitzman 2000; Pollard 2000; Corriveau 2005; Williams et al. 2005).

Recognition of these usually big footprints associated with a mineralization not only help to understand the deposit's character, but also is the key to unlock the wealth of economic mineralization has not been discovered yet (Cudahy et al. 2008). This style of mineralization shows a direct relationship with large scale faults and broad zones of sodium calcium (albite-actinolite) or potassic (K-feldspar or biotite) alteration. Their lithological hosts and ages are non-diagnostic but their alteration zones are, with calcic-sodic regional alteration at deep levels, superimposed by potassic and sericitic alterations.

The results of alteration study in XIV deposit show that wall rock alteration including chlorite, sericite, muscovite and lesser biotite minerals was formed simultaneously in vicinity of them. Subsequent surficial weathering oxidized the magnetite, pyrite and other sulfides to hematite, goethite and jarosite

4. False Color Composite (FCC)

ASTER false color composite 468 (RGB) images typically show argillic and phyllic altered rocks as red tones, and propylitic altered rocks as green tones due to Al–O–H (minerals such as kaolinite, muscovite, montmorilonite and illite, major minerals for phyllic and argillic alteration zones) (centered at ASTER band 6) and Fe–, Mg–O–H (minerals such as chlorite and epidote that are remarkable for propylitic alteration zones) (centered at ASTER band 8) absorption features, respectively (Tommaso and Rubinstein 2007; Mars 2010). The false color composition RGB: 468 for the study area shows the alteration halo enhanced in two different color zones, the phyllic and argillic altered rocks with light red to pink color, and the propylitic altered rocks with green color (Figure 2).

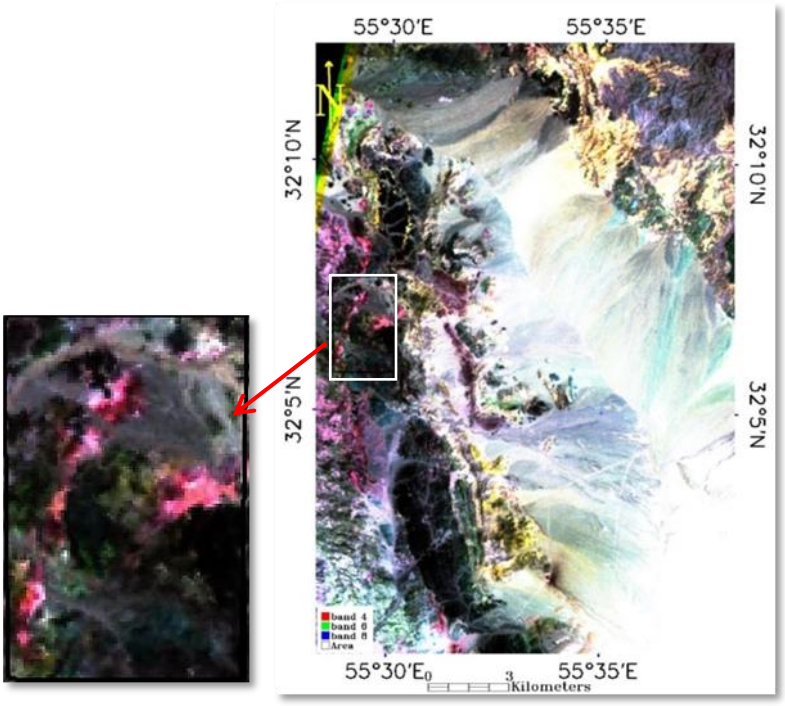

Figure 2. False-color composite in RGB mode (R = 4, G = 6, B = 8). In this color composite, propylitic alteration appears as green, and phyllic and arjillic alteration zones with large quantities of Al-OH minerals are Red to pink in color

5. Band Ratio Method

The band ratioing is the most common technique used to identify and map different lithologies and alteration zones (Arvidson 1986; Rokos et al. 2000; Sultan and Xu et al. 2004; Madani et al. 2008; Mokhtari et al. 2016). Ratio images designed to display the spectral contrast of specific absorption features, have been used extensively in geologic remote sensing (Cudahy et al. 2008; Rowan et al. 1977, 2006; Tommaso and Rubinstein 2007). Image spectral reflectance of alunite, muscovite and kaoline, as well as jarosite, shows absorption features in bands 5, 6 (Al–O–H absorption), and 7 (Fe–O–H absorption), respectively; therefore, band ratio transformation RGB: 4/5, 4/6, and 4/7 (Fig3) highlights the jarositic phyllic and argillic altered rocks in white to yellowish color and the areas underlain by Kiruna mineralization within the white regions.

The band ratio transformation RGB: 4/6, 5/8, and 3/4 (Fig4) is also useful for discriminating among different lithologies present. In this false color view, three main units can be discriminated in the study area: (1) a red zone, having high 4/6 band ratio values, which indicates the presence of muscovite and clay minerals and coincides with outcrops of the of intrusions (granite Zarigan type) and volcano-sedimentary unite as well as felsic–intermediate volcanic and pyroclastic rocks; (2) a green zone, having high 5/8 band ratio values, which reflects the presence of regionally extensive secondary chlorite, epidote and calcite phases. This zone corresponds mainly with propylitic alteration of the cambrian volcanic-sedimentary rocks (Rizu and Dezu series) that surround the intrusive bodies; and (3) a blue zone, having high 3/4 band ratio values, which shows unaltered rocks. This band ratio diagram also highlights the observation a core area that includes the phyllic and argillic alteration zones and hosts the Kiruna deposits, as verified by field investigations. In addition, particularly in the central, the areas of phyllic and argillic alteration define NE-SW trending corridors that likely reflect a structural

control for the hydrothermal fluids that caused this alteration.

6. Relative Band Depth (RBD) Method

Relative band depth (RBD) images are useful for displaying the intensities of Al–O–H, Fe–, Mg–O–H, and CO3 absorption (Crowley et al. 1989; Rowan and Mars 2003; Pazand et al. 2016). The RBD is defined by the ratio among the sum of the bands at the shoulders of a defined absorption peak and the band closest to the peak itself (Crowley et al. 1989; Mars and Rowan 2006). The following RBD images are calculated: (1) RBD4 [(band 3+band 5)/(band 4) ∗ 2], used for detecting volcanic and sedimentary rocks. The laboratory spectral signatures of some volcanic and sedimentary rocks (andesite, siltstone and sandstone) from the ASTER spectral library show absorption features in band 4.; (2) RBD5 [(band 4 + band 6)/(band 5) ∗ 2] and RBD6 [(band 4+band 7)/(band 6) ∗ 2] for detecting Al–O–H absorption in muscovite and clay minerals; however, the RBD6 is better for detecting muscovite; and (3) the RBD8 [(band 7 + band 9)/(band 8) ∗ 2] is focused on Fe–, Mg–O–H and CO3 absorption and is used for delineating chlorite, epidote and carbonates.

In the study area, the RGB false color composed of RBD 6, RBD 8 and RBD 4 confirmed the result of band ratio transformation 4/6, 5/8, and 3/4, as is shown in Fig4, and highlights both the areas of phyllic and propylitic alterations, and unaltered volcanic and pyroclastic rocks. In the RGB false color composite of RBD 5, RBD 6 and RBD 4 (Fig5), four main unit could be discriminated: (1) a yellow to light green zone, which includes high RBD 5 and RBD 6 values, which indicates the presence of muscovite and clay minerals and that is consistent with the alteration of intrusive rocks (granite Zarigan), as well as volcanic and pyroclastic rocks. Note that Kiruna mineralization underlies this area; (2) a dark blue color, which indicates the presence of mainly chlorite, epidote, and minor calcite, and reflects the propylitic alteration of volcanic and pyroclastic rocks (3) a light blue zone with high RBD 4 values, which is coincident with outcrops of unaltered volcanic and pyroclastic rocks. Similar to yellow zone, these dark blue areas also define northeast-trending corridors; and (4) and a dark green zone that is mainly related to the presence of carbonates (CO3) in the propylitically altered rocks, and which is confined to areas underlain by sedimentary rocks (cambrian, volcano-sedimentary unite formations in Figure 1)

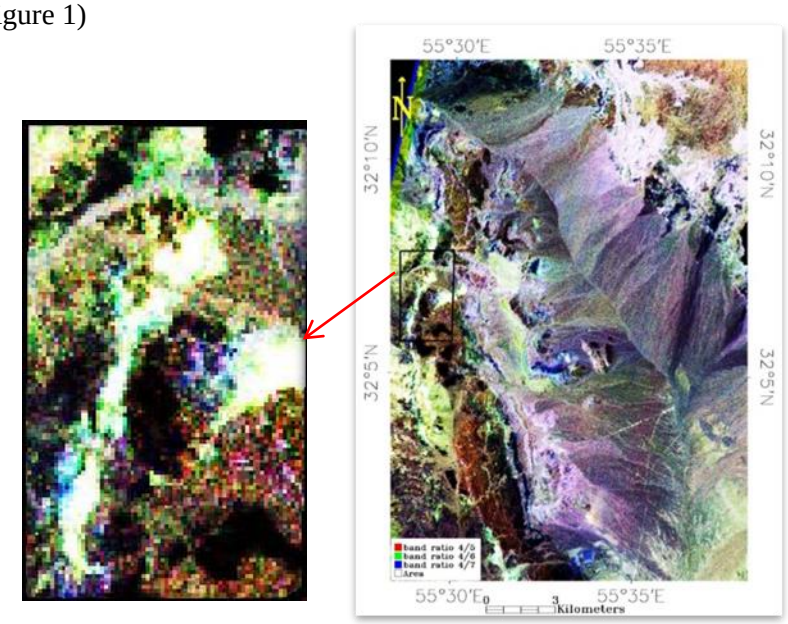

Figure 3. ASTER band ratio values 4/5, 4/6, and 4/7 shown on the XIV anomalies area. The areas underlain by white (to yellowish) show a response of band 5 and band 6 (Al–OHabsorption) and band 7 (Fe– OH absorption) which highlights jarositic phyllic and argillic alterations associated with Kiruna mineralization

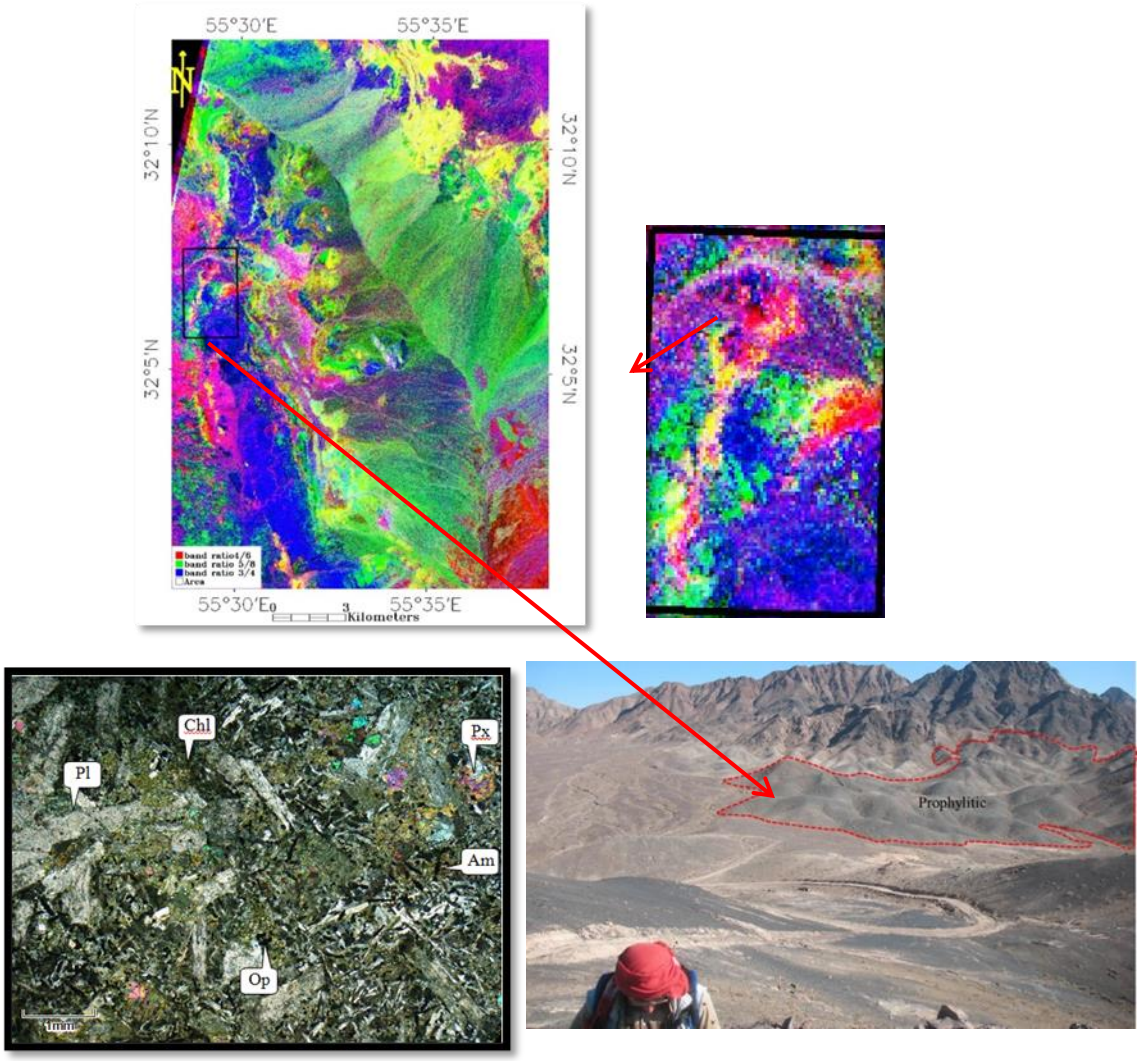

Figure 4. (a) ASTER band ratio values 4/6, 5/8, and 3/4 shown on the XIV anomalies area. In this view of false colors, three main units can be discriminated: A red zone with high 4/6 band ratio values, indicating the presence of muscovite and clayminerals; a green zone with high 5/8 band ratio values, indicating the presence of chlorite–epidote and calcite; and a blue zone with high 3/4 band ratio values, showing unaltered basement rocks. (b) The view of propylitic alteration (in dark). (c) Thin section of gabbro with Plagioclase phenocrysts (pl), pyroxene (Px), amphibole (Am) and chlorite (Chl), together with opaque minerals (XPL: cross polarized light)

7. Minimum Noise Fraction (MNF) Method

MNF is a method similar to principal components used to segregate noise in the data, determine inherent data dimensionality, and reduce computational requirements for subsequent processing (Green et al 1988; Boardman and Kruse 1994; Beiranvnd et al. 2011; Papadaki et al. 2011; Pazand et al. 2016). For hyper spectral data (less-so for multispectral data), the MNF involves two parts; one with large eigenvalues and coherent eigen images and the second with near-unity eigenvalues and noise-dominated images (Weldemariam et al. 2009). It is used as a preparatory transformation to put most of

the interesting information into just a few spectral bands and to order those bands from most interesting to least interesting.

By applying these methods on VNIR and SWIR bands for ASTER, 9 bands created. MNF bands 3, 6, 4 and 7 were used for iron oxide, argillic, phyllic, propylitic and silica alterations. By surveying of bands show MNF2 is suitable propylitic alteration whit white color and argillic alteration with black color. MNF4 is white for argillic alteration (Fig6).

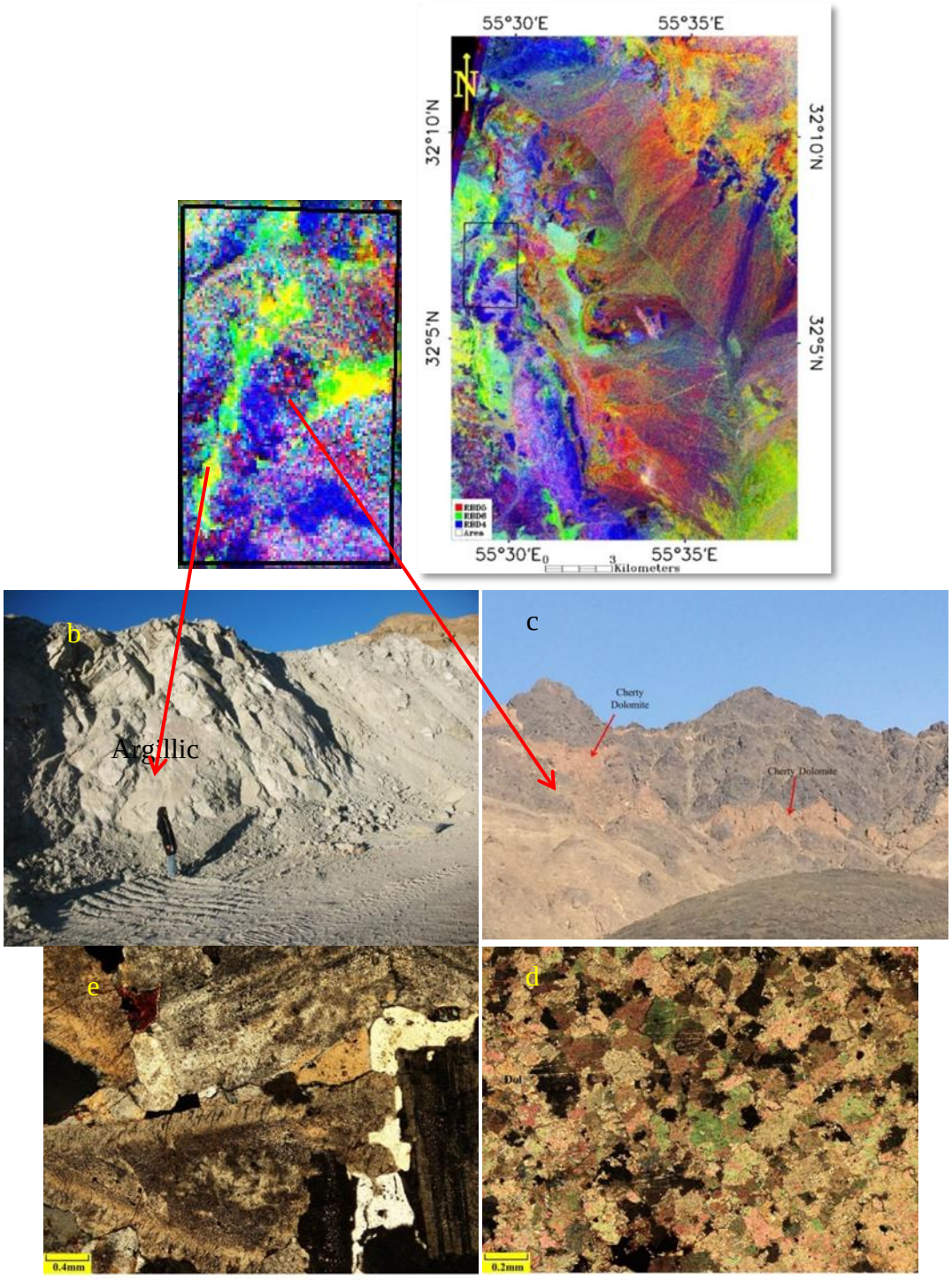

Figure 5. (a) The RGB false color composite of RBD5, RBD6 and RBD4 shown on the XIV anomalies area. The false colors show consistent results for lithologic discrimination, and four main units are distinguished: (1) a yellow to light green zone with high RBD 5 and RBD 6 values, indicating the presence of muscovite and clay minerals; (2) a dark blue color indicating the presence of mainly chlorite–epidote; (3) a light blue zone with high RBD 4 values, showing unaltered volcanic-sedimentary rocks; and (4) a dark green color mainly related to the presence of carbonates (CO3) in propylitic alteration and in the sedimentary rocks. Note that the results are in good agreement with the geological map in Fig1. (b) The view of argilic alteration. (c) The view of carbonate rock. (d) Thin section of carbonate rock (XPL: cross polarized light). (e) Thin section of granit rock (with argillic and philic alteration) with Plagioclase phenocrysts (XPL: cross polarized light)

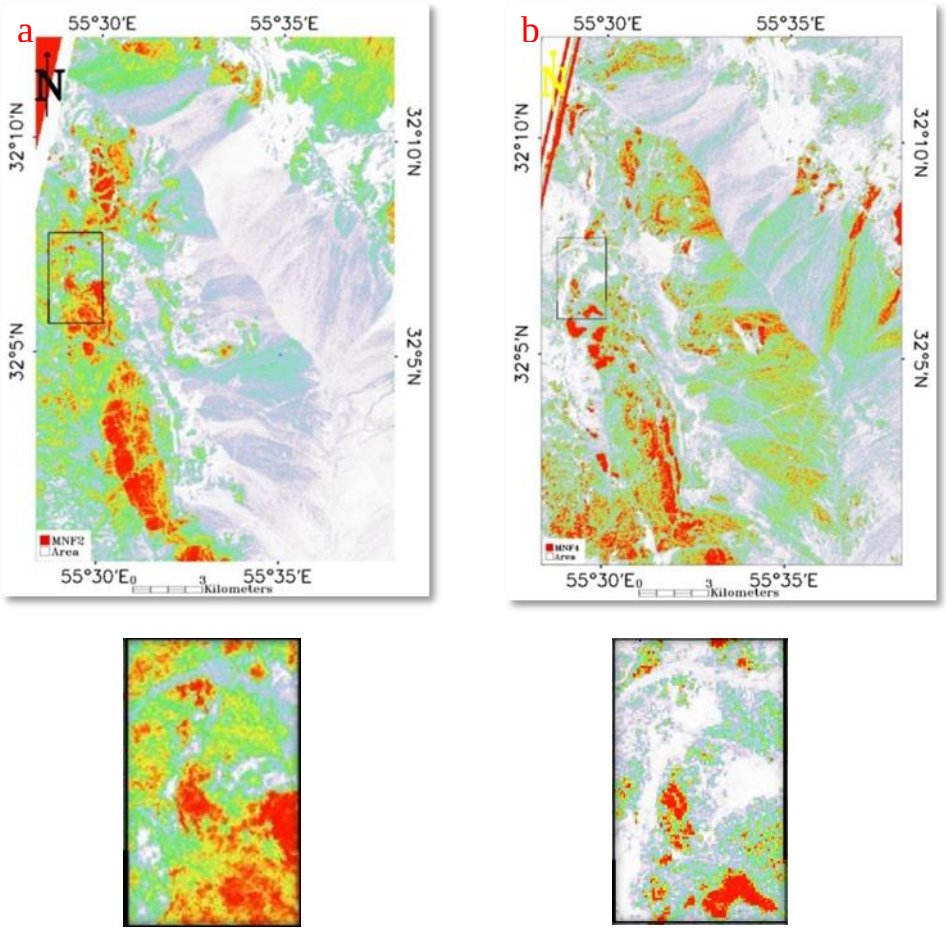

Figure 6. MNF output bands. (a) propylitic alteration appears as red in MNF2 and (b) argillic alteration appears as white in MNF4

8. Principal Component Analysis (PCA) Method

Principal component analysis (PCA) is used to produce uncorrelated output bands, to segregate noise components, and to reduce the dimensionality of data sets. This is applied by finding a new set of orthogonal axes that have their origin at the data mean and that are rotated so that the data variance is

maximized. It is possible to calculate the same number of output PCA bands as input spectral bands. The first PCA band contains the largest percentage of data variance and the second PCA band contains the second largest data variance, and so on; the last PCA bands appear noisy because they contain very little variance, much of which is due to noise in the original spectral data (Crosta et al. 2003).

Principal components bands produce more colorful color composite images than spectral color composite images because the data is uncorrelated. ENVI can complete forward and inverse PC rotations. PC(1,4,5,7) were used for argilic alteration and static result show that PC4 should be inverse. PC(2,5,8,9) were used for epidote and static result show that PC2 should be normal. Finally, PC(2,5,8,9) were used for chlorite and static result show that PC4 should be inverse (epidote and chlorite show propylitic alteration) (Fig7).

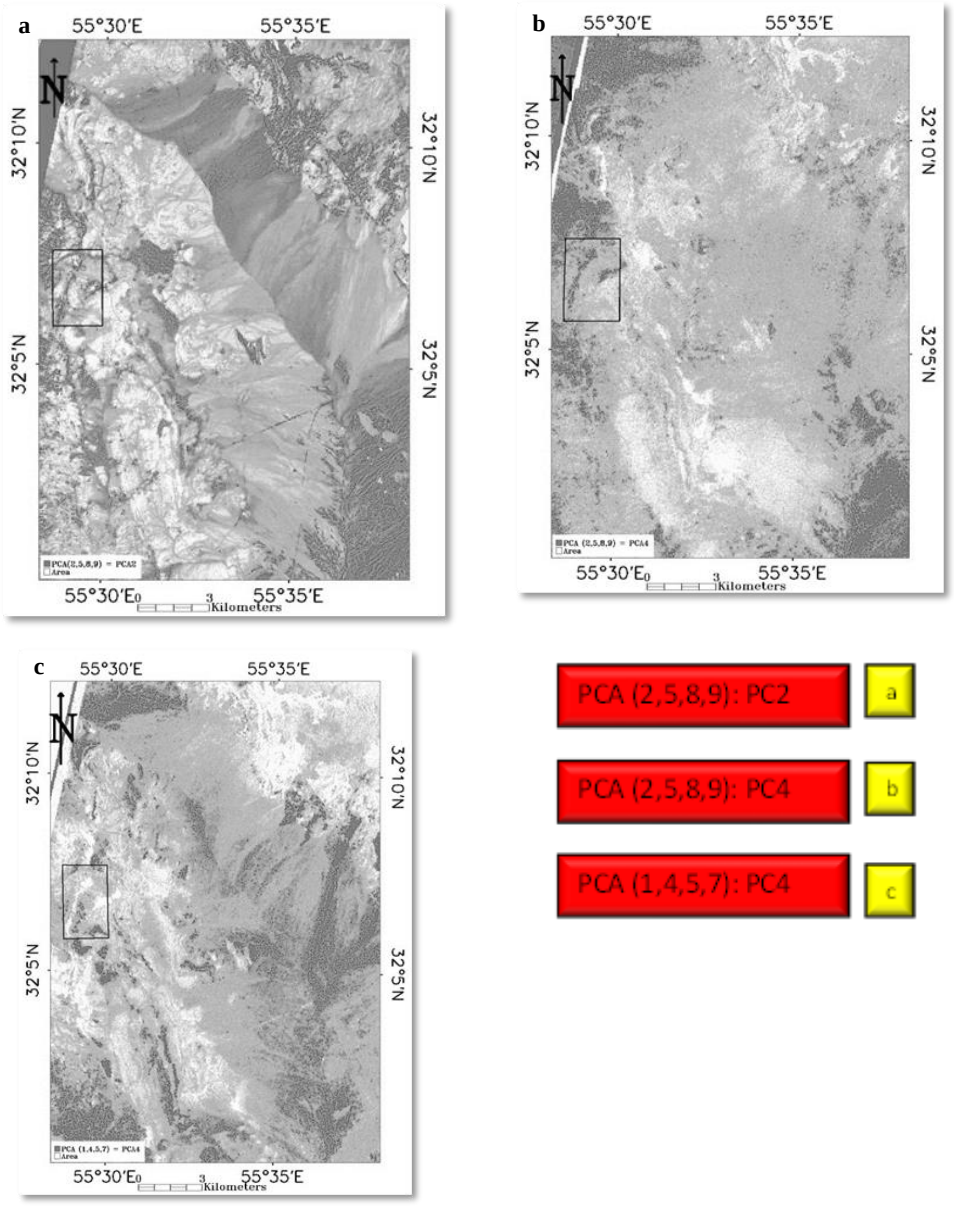

Figure 7. The images prepared based on PCA method a: argillic alteration, b: epidote and c: chlorite

9. Least Square Fitting (LS-Fit)

The technique assumes that the bands used as input values are behaving as the variables of a linear expression and the "y" value of the equation, namely the predicted band information, gives us a calculated output value. This predicted band is what that band should be according to the linear equation. The minerals which are sensitive to a specific band are then differentiated from the features which are reflective to the other bands as well; just by taking the difference between the predicted values and the original values (Sarp 2005). Distribution of iron oxide was created by using all the 3 visible and near-infrared (VNIR) bands as the input bands and VNIR-b1 as the modeled band also, argillic, phyllic and propylitic alterations were mapped by using residual band SWIR-b4, residual band SWIR-b6 and residual SWIR-b9 (Fig8).

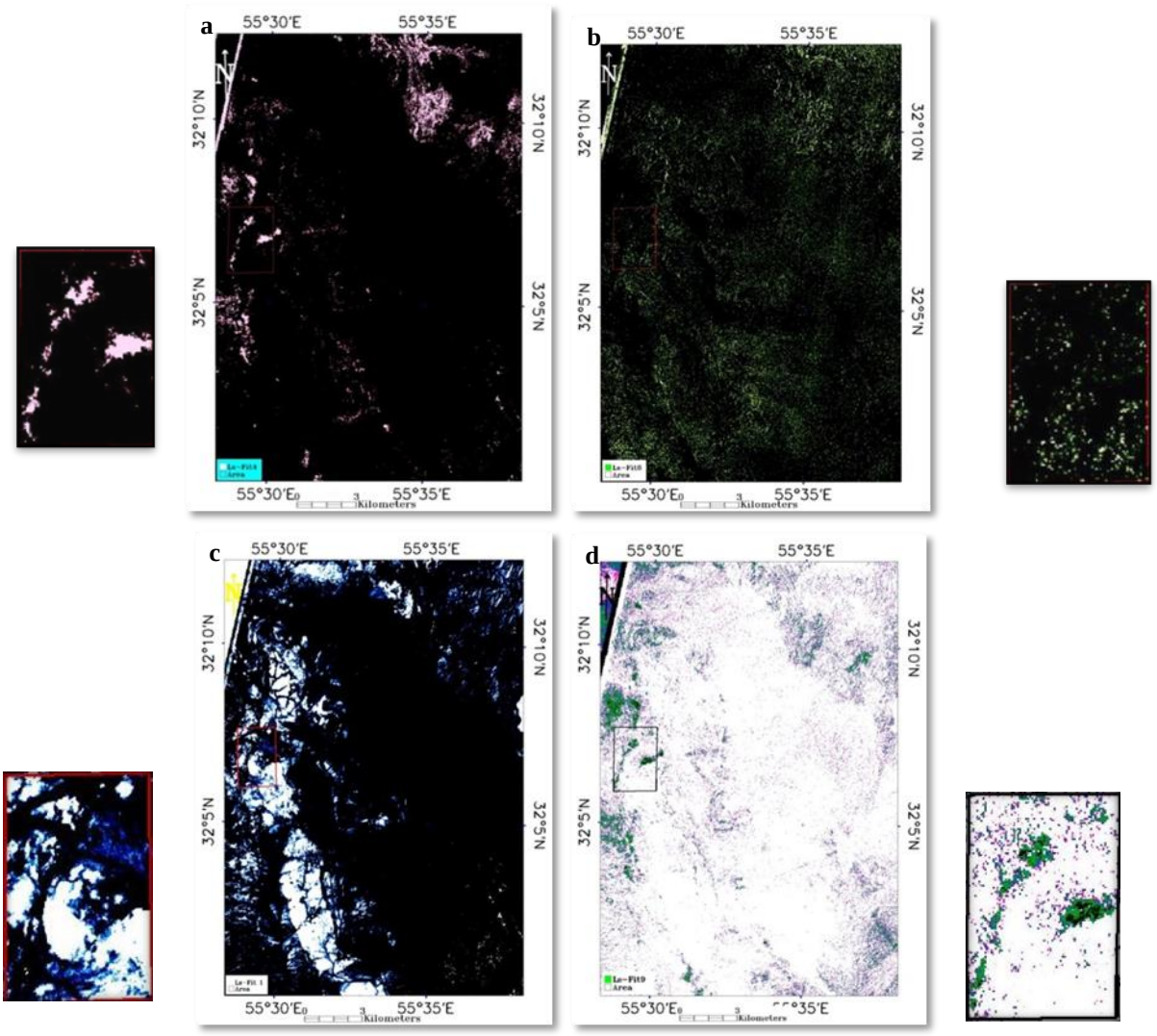

Figure 8. (a) The phyllic (LS- Fit6), (b) argillic (LS- Fit4), (c) iron oxide (LS- Fit1) and (d) propylitic (LS- Fit9) images prepared based on Ls-Fit method

10. ASTER TIR Data Analysis

Mapped in the 5 thermal-infrared (TIR) bands by using the quartz (Qi) index (Ninomiya, 2003). This factor Qi, is expected to be high for quartz and low for K-feldspar (inverse Qi) (Ninomiya et al. 2005). Some desired and almost pure pixels for quartz were extracted from the Qi-image and subsequently used to map the distribution of silicified rocks in the study area (Fig. 9). Hydrothermally altered silica-rich rocks associated with Kiruna consist primarily of quartz veins, silica lithocaps, or silicified materials (Titley 1972; Sillitoe 1995, 2010). In the XIV anomalies area, quartz-bearing rocks include both intrusive bodies and silicified rocks. The ASTER TIR band passes were useful in detecting the silicic alteration. The areas of silica enrichment follow the patterns of other alteration types noted above, and define a northwest trending linear structure that is spatially coincident with the presence of mineralized centers.

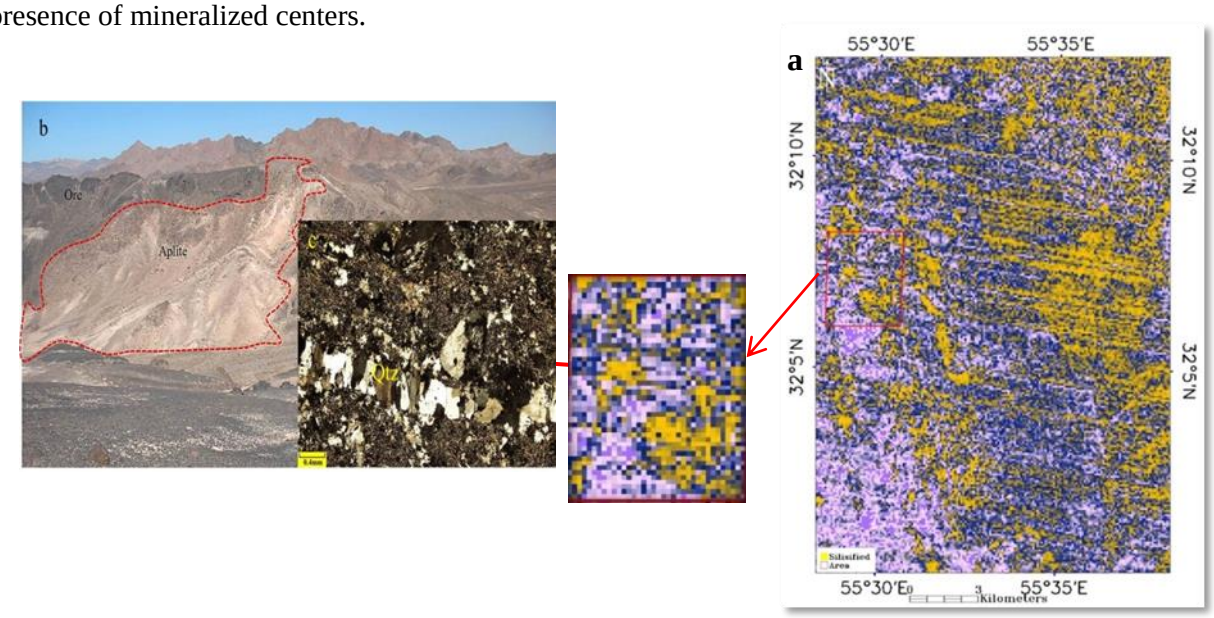

Figure 9. (a) Mineral map showing the results of Qi method using ASTER TIR data to detect silicified rocks in XIV anomalies area which is overlain on an ASTER PCA1 graytone image. The yellow color shown the silicified alteration zones. (b) The view of silisified alteration (in light color). (e) Thin section of granit rock (with silicified alteration) with quartz phenocrysts in vein (XPL: cross polarized light)

11. Pixel Purity Index (PPI) and N-D Visualize Method

The pixel purity index (PPI) is used to find the most spectrally pure (extreme) pixels in multispectral and hyperspectral images (Boardman and Kruse 1994). These typically correspond to mixing end members. The PPI is computed by repeatedly projecting n-d scatter plots on a random unit vector. ENVI records the extreme pixels in each projection (those pixels that fall onto the ends of the unit vector) and it notes the total number of times each pixel is marked as extreme. A pixel purity image is created where each pixel value corresponds to the number of

times that pixel was recorded as extreme.

The PPI function can create a new output band or continue its iterations and add the results to an existing output band. The PPI is typically run on an MNF transform result, excluding the noise bands (see minimum noise fraction transform) (Azizi et al. 2009). Whatever the iteration will be more, there would be better results in this method. The iteration is 10000 time in this project (fig10). According to our diagram and images and comparing with classing that were used, we conclusion, in southern and

western of studied area pure pixel were observed that would be suitable for alteration areas. With comparison to former methods or N-D visual and pixels classing can be determined alteration areas (Fig11).

After calculation of the PPI, the N-D visualizer was used in conjunction with the MNF and PPI results to locate, identify, and cluster the purest pixels and most extreme spectral responses in the data set. The N-D visualizer is an interactive tool for selection of the end members in n-space (Fig12). With using this method, the especial pixels were classified and then these classes compared with the alteration minerals in United States Geological Survey library. At last the alteration zones were distinguished.

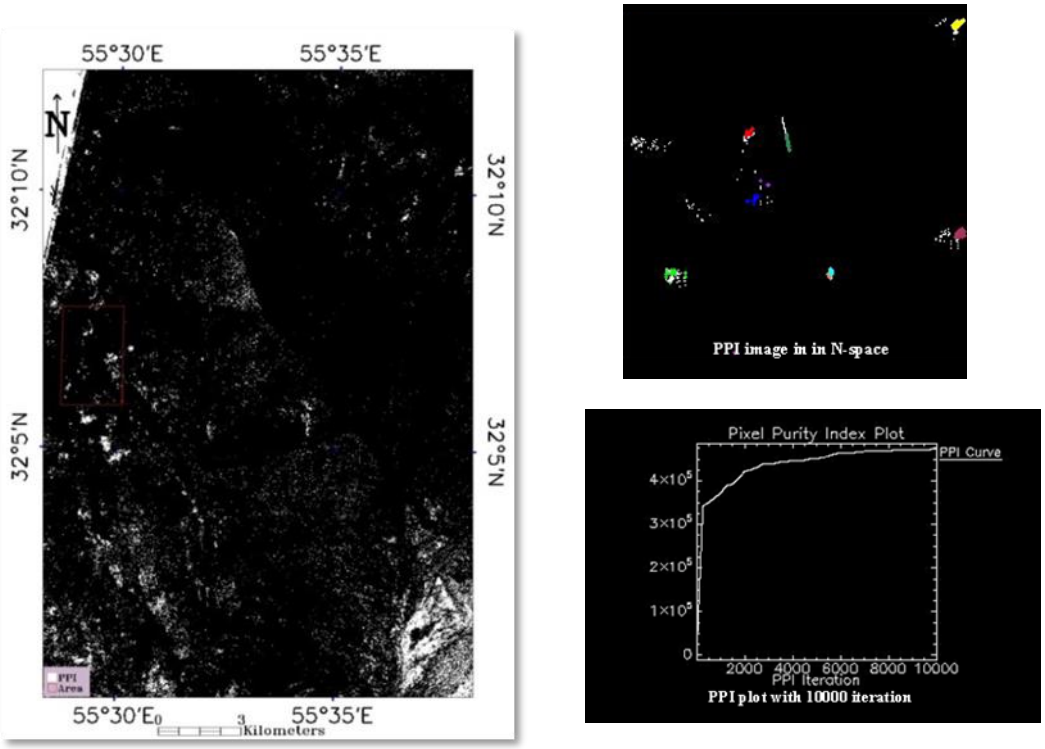

Figure 10. Pure pixel were observed in white color especially in western and eastern of the area (XIV anomalies shown with rectangle)

12. Discussion

Remote sensing is a proper method for primary exploration process and useful for advanced exploration, particularly in the surface of deposit in order to recognize the hydrothermal fluid effects as alteration. In this study, ASTER satellite data was used to map the altration and mineralogical evidences of XIV Kiruna mineralization by visual image interpretation and spectral processing techniques, respectively. The outcomes of this study have been compared by field and laboratory observations.

Subsequent field checking and microscopic study indicated the accuracy of these remotely mapped minerals and hence confirming the utilized hybrid processing algorithms.

- Image processing with RGB:468 has shown The propylitic alteration zone is located in central and south part of the area and the phillic alteration zones are very poor in northwest, northeast and

southwest.

- Ratio image, relative band depth (RBD) and MNF methods has shown that The propylitic, phillic and argillic alterations zone is overlapping with previous method.

-PPI method has completed the MNF and has separated argillic and propylitic alteration zones based on pure pixels.

-PCA method has shown argillic alteration zones in northwest but it doesn't have shown the philic alteration around the main drainage and it was disseminated. Also this method confirmed the propylitic alteration zone in center and south of the area.

-The processing with ASTER TIR analysis for sillisified zones has shown some disseminated places especially in northwest and southeast of the area.

- the processing with RBD methods This method for The argillic and phillic alteration zones has shown around the main drainage, northwast corner and a place in east of the area. This method for the propylitic alteration zones is overlapping with previous methods completely.

Sheikhrahimi in a research, Sanandaj-Sirjan region (SSZ) as an important area for gold exploration in the western part of Iran, which costs mining companies that implement new exploration programs. In this research, ASTER is used for mapping of hydrothermal alteration minerals and better detection of geological structural features related to orogenic gold in the region. Image conversion techniques such as specialized banding and principal component analysis are used to characterize lithological units and alteration minerals. Monitoring-based classification techniques, namely spatial surveying (SAM) and information dependence (SID) are used to detect differences between mineralogy change indicators associated with gold sites in the region. The filter technique is used to help trace along the strike of various line structures. The results show that the integration of image conversion and classification techniques of ASTER data monitoring with field exploration and geochemical studies is very effective in targeting new gold mineralization prospects in SSZ (Sheikhrahimi, et al, 2019).In a study, the Neuro-Fuzzy-AHP (NFAHP) technique was used to combine remote sensing (e.g., ASTER transformation mineral image maps) and geological datasets to identify high potential areas of volcanic massive copper sulfide (VMS) mineralization. It was developed in Sahlabad mine area, east of Iran. Argillic, phyllic, propylitic, and gasan alteration zones were identified in the study area using band ratio methods and selected principal component analysis (SPCA) for ASTER VNIR and SWIR bands. In conclusion, Neuro-Fuzzy-AHP (NFAHP) technique shows high reliability for copper exploration in Sahlabad mining area (Shirazi et al, 2022). In a study, Mori et al. evaluated data from the Advanced Spatial Thermal and Reflectance Radiometer for gold and base metal mineralization mapping through variational mapping. Two different methods of selective principal component analysis and matched filter processing were used to map argillic and siliceous changes. By using the spectral library and the laboratory spectrum of the samples of the studied area, similar results were obtained. However, MF, using image reference spectra from principal component (PC) images, produced the best results, demonstrating the advantage of using image spectra instead of library spectra in spectral mapping techniques. Argillic alteration seems to be more effective than siliceous alteration for exploration purposes. (Moore et al (2008).

With comparing all above results and with taking into consideration the lithological situation and overlapping the result of different methods we should choose the especial places with more overlapping for every alteration because all of the methods will not confirm each other and it is possible that some of them give the wrong results.

13. Conclusions

The use and application of VNIR+SWIR ASTER data for mapping the regional extent of hydrothermal alteration in the part of Ariz sheet of Iran, including a more detailed analysis of the highly prospective Bafq district, are accurate and helpful in detecting and mapping out extensive zones of phyllic, argillic and propylitic alteration, and also Fe-oxides/hydroxides. In addition, TIR emissivity analysis is useful for distinguishing and mapping out silicic alteration, with the most promising results

obtained by the matched filter processing technique. The results of this study indicate the presence of extensive phyllic, argillic, propylitic and silicic alteration zones. The distribution of the alteration patterns highlights the role of regional structures in localizing fluid flow, an integral part of Kiruna deposit formation. Furthermore, the analysis of ASTER TIR data also show that silicic alteration, which is not generally discussed as a common alteration feature in Kiruna systems (Hitzman 2000; Pollard 2000; Corriveau 2005; Williams et al. 2005) tends to be associated with the Kiruna type mineralization in the well mineralized XIV anomalies area. In summary, the results of this study confirm that ASTER images can be a useful and powerful tool in the initial steps of exploration for those deposit types where large alteration zones are an integral part of the deposit model because these data provide highly accurate and reliable information about the distribution of alteration minerals.

References

Abdelsalam, M.G., Stern, R.J., & Berhane, W.G. (2000). Mapping gossans in arid regions with Landsat TMand SIR-C images: the Beddaho Alteration Zone in northern Eritrea. *J. Afr. Earth Sci*. 30 (4), 903–916.

Aita, S. K., & Omar, A. E. (2021). Exploration of uranium and mineral deposits using remote sensing data and GIS applications, Serbal area, Southwestern Sinai, Egypt. *Arabian Journal of Geosciences*, *14*, 1-17.

Azizi, H., Mehrabi, B., & Akbarpour, A. (2009). Genesis of tertiary magnetite apatite deposits, southeast of Zanjan, Iran. *Resour. Geol*. 59, 330–341.

Beiranvnd Pour, A., & Hashim, M. (2012). Identifying areas of high economic-potential copper mineralization using ASTER data in the Urumieh–Dokhtar Volcanic Belt, Iran. *Adv. Space Res*. 49 (4), 753–769.

Beiranvnd Pour, A., Hashim, M., & Marghany, M. (2011). Using Spec tral Mapping Techniques on Short Wave Infrared Bands of ASTER Remote Sensing Data for Alteration Mineral Mapping in SE Iran, *International Journal of the Physical Sciences*, 6(4), 917-929.

Bhadra, B. K., Pathak, S., Karunakar, G., & Sharma, J.R. (2016). ASTER Data Analysis for Mineral Potential Mapping Around Sawar-Malpura Area, Central Rajasthan. *Journal of the Indian Society of Remote Sensing* 41(2) , 391-404

Boardman, J. W., & Kruse, F. A. (1994). Automated spectral analysis: a geologic example using AVIRIS data, north Grapevine Mountains, Nevada. *Proceedings of the Tenth Thematic Conference on Geologic Remote Sensing* (pp. I407 – I418). Ann Arbor: Environ. Res. Inst. Of Michigan.

Borook D.M., Kesler S.E., Boer R.H. & Essene E.J. (1998). The Vergenoeg magnetite-fluorite deposit, South Africa: support for a hydrothermal model for massive iron oxide deposits. *Economic Geology*, **93**, 564-586.

Corriveau, L. (2005). Iron Oxide copper-gold (+/-Ag,+/-Nb,+/-REE,+/-U) deposits: A Canadian Perspective: *Geological Survey of Canada*, Open File, 1-23.

Crósta, A.P., & Filho, C.R.d.S. (2003). Searching for gold with ASTER. Earth Obs. Mag. 12 (5), 38–41.

Crósta, A.P., & Moore, M.J. (1989). Enhancement of Landsat Thematic Mapper imagery for residual soil mapping in SW Minas Gerais State Brazil: a prospecting case history in greenstone belt terrain. *9th Thematic Conference on Remote Sensing for Exploration Geology. Environmental Research Institute of Michigan, Ann Arbor*, 1173–1187.

Crowley, J.K., Brickey, D.W., & Rowan, L.C. (1989). Airborne imaging spectrometer data of the Ruby Mountains, Montana: mineral discrimination using relative absorption band depth images. *Remote Sens. Environ*. 29, 121–134.

Cudahy, T., Jones, M., Thomas, M., Laukamp, C., Caccetta, M., Hewson, R., Verrall, M., Hacket, A., & Rodger, A. (2008). Mineral mapping Queensland: iron oxide copper gold (IOCG) mineral system case history, Starra, Mount Isa Inlier, PACRIM Congress 2008,: *Gold Coast, QLD, Australia*, 153–160.

Eldosouky, A. M., El-Qassas, R. A., Pour, A. B., Mohamed, H., & Sekandari, M. (2021). Integration of ASTER satellite imagery and 3D inversion of aeromagnetic data for deep mineral exploration. *Advances in Space Research*, *68*(9), 3641-3662.

Ferrier, G., & Wadge, G. (1996). Application of imaging spectrometry data to mapping alteration zones associated with gold mineralization in southern Spain. *International Journal of Remote Sensing* 17, 331–350.

Ferrier, G., White, K., Griffiths, G., & Bryant, R. (2002). The mapping of hydrothermal alteration zones on the island of Lesvos, Greece using an integrated remote sensing dataset. *Int. J. Remote. Sens*. 23, 341–356

Forster, H., & Jafarzadeh, A. (1994). The Bafq mining district in central Iran – a highly mineralized Infracambrian volcanic field. *Economic Geology* 89, 1697–1721.

Frietsch, R. (1978). On the magmatic origin of the iron ores of the Kiruna-type. Ibid., **73**, 478-485.

Gabr, S., Ghulam, A., Kusky, T., (2010). Detecting areas of high potential gold mineralization using ASTER data. *Ore Depos. Rev*., 38, 59–69.

Green, A. A., Berman, M., Switzer, P., & Craig, M. D. (1988). A Transformation for Ordering Multispectral Data in Terms of Image Quality with Implications for Noise Removal, *IEEE Transactions on Geoscience and Remote Sen* 26 (1), 65-74.

Haghipour, A. (1977). Geological Map of Posht-e-Badam Area. Geol. Surv. Iran.

Hegab, M. A. E. R., Mousa, S. E., Salem, S. M., Farag, K., & GabAllah, H. (2022). Gold-related Alteration Zones Detection at the Um Balad Area, Egyptian Eastern Desert, using Remote Sensing, Geophysical, and GIS Data Analysis. *Journal of African Earth Sciences*, *196*, 104715.

Hitzman, M.W. (2000). Iron oxide-Cu-Au deposits: what, where, when, and why, in Porter, T.M. ed., Hydrothermal iron oxide copper-gold & related deposits: A global perspective: P*GE Publishing, Adelaide*, 1, 9-25.

Hitzman, M.W., Oreskes, N., & Enaudi, M. (1992). Geological characteristics and tectonic setting of Proterozoic iron oxide (Cu-U-Au-REE) deposits. *Precambrian Research* 58, 241–287.

Hunt, G.R. (1977). Spectral signatures of particulate minerals in the visible and near infrared. *Geophysics* 42, 501–513.

Loughlin,W.P. (1991). Principal component analysis for alteration mapping. Photogramm. *Eng. Remote. Sens.* 57, 1163–1169.

Madani, A., Harbi, H., & Eldougdoug, A. (2008). Utilization of remote sensing techniques for mapping the listwaenite associated with Jabal Al-Wask Ophiolite Complex, Northwestern Saudi Arabia. Egypt. *J. Remote. Sens*. & Space Sci. 11, 57–72.

Mars, J.C. (2010). VINR-SWIR and TIR remote sensing of porphyry copper deposits. In: John, D.A. (Ed.), Porphyry Copper Deposit Model. *Scientific Investigations Report 2010*- 5070-B, 38–50.

Mars, J.C., & Rowan, L.C. (2006). Regional mapping of phyllic and argillic altered rocks in the Zagros magmatic arc, Iran, using Advanced Spaceborne Thermal Emission and Reflection Radiometer (ASTER) data and logical operator algorithms. *Geosphere* 2, 161–186.

Mokhtari, Z., Boomeri, M., & Bagheri, S. (2016). Digital Image Processing and Analysis Techniques for Detection of Hydrothermal Alteration Zones: A Case Study in SiahJangal Area, North of Taftan Volcano, Southeastern Iran. *Journal of the Indian Society of Remote Sensing*. 43(2), 363-377

Moore, F., Rastmanesh, F., Asadi, H., & Modabberi, S. (2008). Mapping mineralogical alteration using principal-component analysis and matched filter processing in the Takab area, north-west Iran, from ASTER data. *International Journal of Remote Sensing*, *29*(10), 2851-2867.

Ninomiya, Y., (2003). Rock typemapping with indices defined for multispectral thermal infrared ASTER data: case studies. Proc. SPIE Int. Soc. Opt. *En*g. 4886, 123–132.

Ninomiya, N., Fu, B., & Cudahy, T.J. (2005). Detecting lithology with Advanced Spaceborne Thermal and Reflection Radiometer (ASTER) multispectral thermal infrared "radiance- at-sensor" data. *Remote Sens. Environ*. 99, 127–135.

Nyström, J.O., & Henriquez, F., (1994). Magmatic features of iron ores of the Kiruna type in Chile and Sweden: ore textures and magnetite geochemistry. *Economic Geology*, **89**, 820-839

Papadaki, S. E. Mertikas, S. P., & Sarris, A., (2011). Identification of Lineaments with Possible Structural Origin Using ASTER Images and DEM Derive Products in Western Crete, GREECE, *European Association of Remote Sensing Laboratories* (ARSeL).

Pazand, K., Fereidoni Sarvestani, J., & Ravasan, M. R. S. (2016). Hydrothermal Alteration Mapping Using ASTER Data for Reconnaissance Porphyry Copper Mineralization in the Ahar Area, NW Iran. *Journal of the Indian Society of Remote Sensing*. 41(2), 379-389.

Pollard, P.J. (2000). Evidence of a magmatic fluid and metal source for Fe-oxide Cu-Au mineralization, in

Porter, T.M. ed., Hydrothermal iron oxide copper-gold & related deposits: A global perspective: *PGC Publishing*, Adelaide, 1, 27-41.

Ramezani, J., & Tucker, R.D. (2003). The Saghand region, Central Iran: U–Pb Geochronology, Petrogenesis and Implications for Gondwana Tectonics. *Am. J. Sci*. 303, 622–665.

Rokos, D., Argialas, D., Mavrantza, R., St.-Seymour, K., Vamvoukakis, C., Kouli, M., Lamera, S., Paraskevas, H., Karfakis, I., & Denes, G. (2000). Structural mapping and analysis for a preliminary investigation of possible gold mineralization by using remote sensing and geochemical techniques in a GIS environment: study area: island of Lesvos, Aegean Sea, Hellas. *Nat. Resour. Res*. 9, 277–293.

Rowan, L.C., Goetz, A.F.H., & Ashley, R.P. (1977). Discrimination of hydrothermally altered and unaltered rocks in visible and near infrared multispectral images. *Geophysics* 42, 522–535.

Rowan, L.C., & Mars, J.C. (2003). Lithologic mapping in the Mountain Pass, California area using Advanced Spaceborne Thermal Emission and Reflection Radiometer (ASTER) data. *Remote Sens. Environ.* 84, 350–366.

Rowan, L.C., Schmidt, R.G., & Mars, J.C. (2006). Distribution of hydrothermally altered rocks in the Reko Diq, Pakistan mineralized area based on spectral analysis of ASTER data. *Remote Sens. Environ*. 104, 74–87.

Rokos, D., Argialas, D., Mavrantza, R., St.-Seymour, K., Vamvoukakis, C., Kouli, M., Lamera, S., Paraskevas, H., Karfakis, I., & Denes, G. (2000). Structural mapping and analysis for a preliminary investigation of possible gold mineralization by using remote sensing and geochemical techniques in a GIS environment: study area: island of Lesvos, Aegean Sea, Hellas. Nat. *Resour. Res*. 9, 277–293.

Sheikhrahimi, A., Pour, A. B., Pradhan, B., & Zoheir, B. (2019). Mapping hydrothermal alteration zones and lineaments associated with orogenic gold mineralization using ASTER data: A case study from the Sanandaj-Sirjan Zone, Iran. *Advances in Space Research*, *63*(10), 3315-3332.

Shirazi, A., Hezarkhani, A., Beiranvand Pour, A., Shirazy, A., & Hashim, M. (2022). Neuro-Fuzzy-AHP (NFAHP) technique for copper exploration using Advanced Spaceborne Thermal Emission and Reflection Radiometer (ASTER) and geological datasets in the Sahlabad mining area, east Iran. *Remote Sensing*, *14*(21), 5562

Sillitoe, R.H. (1995). Exploration of porphyry copper lithocaps. Pacrim Congress 1995 — Exploring the Rim. Australasian Institute of Mining and Metallurgy Publication Series. *Australasian Institute of Mining and Metallurgy, Parkville Victoria*, 527–532.

Sarp, G. (2005). Lineament Analysis from Satellite Images, North- West of Ankara, MASTER of Science Dissertation, *School of Natural and Applied Science of Middle East Technical University*.

Sultan, M., & Arvidson, R.E. (1986). Mapping of serpentinites in the EASTERn Desert of Egypt by using Landsat Thematic Mapper data. J. *Geol*. 14, 995–999.

Titley, S.R. (1972), Intrusion and wall rock porphyry copper deposits. *Econ. Geol. Bull. Soc. Econ. Geol.* 67, 122–123.

Tommaso, I.M., & Rubinstein, N. (2007). Hydrothermal alteration mapping using ASTER data in the Infiernillo porphyry deposit, Argentina. *Ore Geol. Rev*. 32, 275–290.

Weldemariam, A. F. (2009). Mapping Hydrothermally Altered Rocks and Lineament Analysis through Digital Enhancement of ASTER Data Case Study: Kemashi Area, Western Ethiopia, MASTER of Science Dissertation, *Addis Aba- ba University, Addis Ababa*.

Williams, P.J., Barton, M.D., Johnson, D.A., Fontbote, L., Haller, A.D., Mark, G., Oliver, N.H.S., & Marschik, R. (2005). Iron oxide copper-gold deposits: geology, space-time distribution, and possible modes of origin: Economic Geology, *100th Anniversary*, 371-405.

Xu, Y., Lin, Q., Shao, Y., & Wang, L. (2004). Extraction mechanism of alteration zones using ASTER imagery. Geoscience and Remote Sensing Symposium, 2004. IGARSS '04. Proceedings. 2004 *IEEE International*, 6, 4174–4175.

Yetkin, E., Toprak, V,. & Suezen, M. L. (2004). Alteration Mapping by Remote Sensing: Application to Hasandağ-Me- lendiz Volcanic, Complex, *Geo-Imagery Bridging Continents 10th ISPRS Congress, Istanbul.*

Zhang, X., Pazner, M., & Duke, N. (2007). Lithologic and mineral information extraction for gold exploration using ASTER data in the south Chocolate Mountains (California). Photogramm. *Remote. Sens*. 62, 271–282.